

# Preventing Barren Plateaus in Continuous Quantum Generative Models

Olli Hirviniemi,<sup>1,\*</sup> Afrad Basheer,<sup>2,†</sup> and Thomas Cope<sup>2,‡</sup>

<sup>1</sup>*IQM, Keilaranta 19 D, 02150 Espoo, Finland*

<sup>2</sup>*IQM, Georg-Brauchle-Ring 23-25, 80992 München, Germany*

Recent developments in the field of variational quantum circuits (VQCs) have shifted the prerequisites for trainability for many barren plateau-free models onto the data encoding state fed into a classically trainable unitary. By strengthening proofs relating to small-angle initialisation, we provide a full circuit model which does not suffer from barren plateaus and is robust against current classical simulation techniques, specifically tensor network contraction and Pauli propagation. We propose this as a quantum generative model amenable towards NISQ devices and quantum-classical hybrid models, raising new questions in the debate regarding usefulness of VQCs.

## I. INTRODUCTION

### A. Background and Motivation

Ever since the publication of Shor’s seismic algorithm [1], there has been an extensive research effort to understand the additional computational power that quantum systems provide, and build systems to enable this power. Despite their promise, however, the engineering challenges which must be overcome to build quantum computers capable of running large-scale, fault tolerant algorithms remain significant, as so researchers have turned to other algorithms to test the power of our current noisy intermediate scale quantum (NISQ) devices [2]. Of these, one of the most intensely studied areas has been that of *variational algorithms* [3, 4]; in which an ansatz circuit is chosen; and then its parameters variationally optimised to minimise/maximise a desired cost function. Typically these cost functions take the form of linear operators,  $f(\theta) = \text{Tr}[\rho U^\dagger(\theta) O U(\theta)]$ .

One of the areas these models have been applied to is the field of machine learning; in such models there is an additional *encoding* of the data  $\mathbf{x}$  into the state  $\rho(x)$ , so that the cost function takes the form  $\mathbb{E}_{x \sim \mathcal{D}} \text{Tr}[\rho(\mathbf{x}) U^\dagger(\theta) O U(\theta)]$ . This is the general form for such models [5].

One issue with variational methods is, in the absence of prior knowledge regarding how to initialise the variational parameters  $\theta$ , typically one cannot do better than picking a starting point uniformly. It was quickly realised that, for expressive ansätze, this leads to a phenomenon known as *Barren Plateaus* [6–9]. This issue is characterised by the gradient becoming exponentially small over almost all parameter instances; as  $O(1/\varepsilon^2)$  shots are required to estimate an observable up to precision  $\varepsilon$ , this means that even a single update becomes exponentially demanding.

Consequently, several ansätze were proposed which provably do not suffer from barren plateaus, such as shallow hardware efficient circuits [10–17], quantum convolutional neural networks [18] and small angle initialisations [19–21]. In [22] there was a further blow to variational algorithms however, when it was pointed out that most “barren-plateau” free ansätze can be optimised purely classically. These fall into two further categories; either  $f(\theta) = \text{Tr}[\rho U^\dagger(\theta) O U(\theta)]$  can be estimated purely classically; meaning the ansatz is effectively a classical algorithm; or  $f(\theta)$  requires a classical description  $\rho_{\text{classical}}$  of the state  $\rho$  (e.g. classical shadows) which is only attainable through the use of a quantum computer; this still offers the possibility of a quantum advantage.

In the context of quantum machine learning, the transform  $x \rightarrow \rho(x)_{\text{classical}}$  can be thought of a quantum-enabled feature transform; and the final performance of the algorithm depends heavily on not just the choice of encoding  $x \rightarrow \rho(x)$ , but also the distribution of data  $x \sim \mathcal{D}$ . These two factors combined can lead to *both* a barren plateau due to the distribution  $\mathcal{D}$ , but also a fully classical algorithm. It is therefore difficult to talk about the power of a quantum machine learning variational algorithm without explicit reference to the dataset in question.

---

\* [olli.hirviniemi@meetiqm.com](mailto:olli.hirviniemi@meetiqm.com)

† [afrad.basheer@meetiqm.com](mailto:afrad.basheer@meetiqm.com)

‡ [thomas.cope@meetiqm.com](mailto:thomas.cope@meetiqm.com)

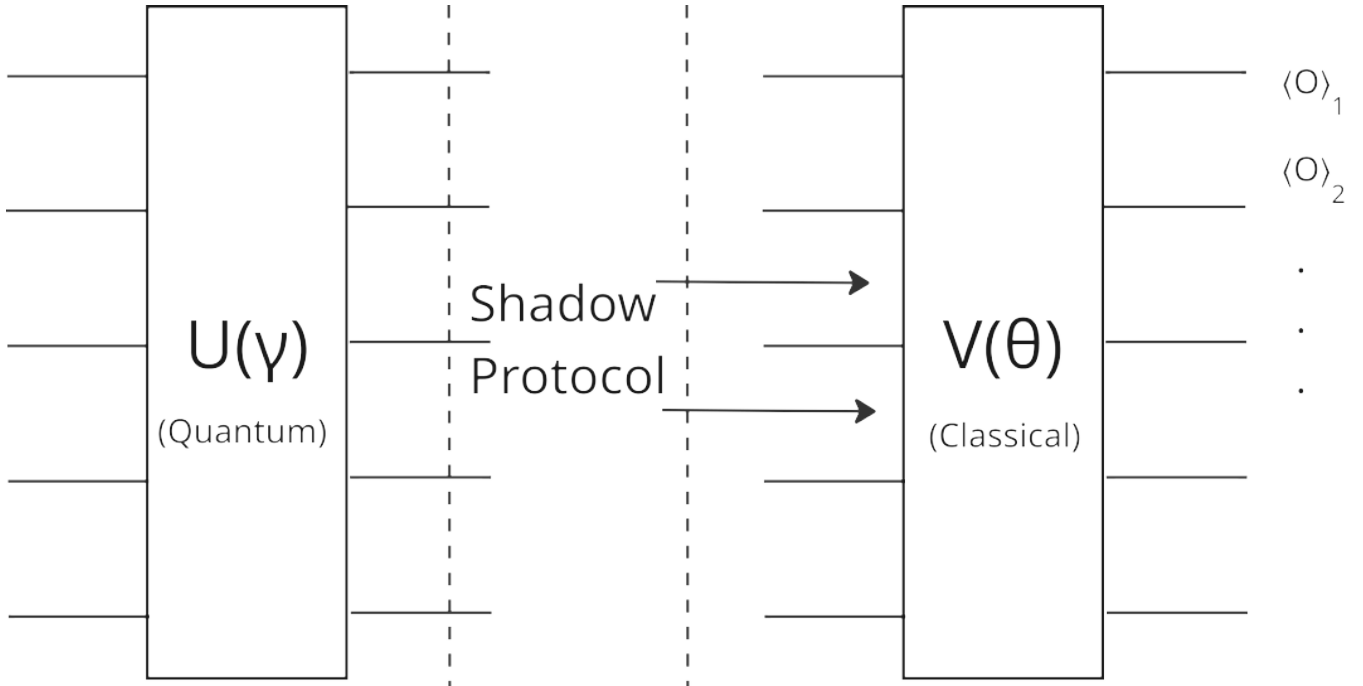


FIG. 1. The proposed structure for a continuous variable quantum generative model. One could also run the full circuit, rather than using classical shadows.

In this paper, we avoid this issue by considering a different machine learning paradigm; that of *generative* learning. In generative machine learning, the goal is not to simply learn a function of the data  $f(x)$ , but to produce new data samples. This is done by learning, and then sampling, from the target data distribution  $\mathcal{D}$ . By substituting into the encoding part of the circuit a known distribution  $\gamma \sim \Gamma$ , we obtain a trainable distribution consisting of features  $(\text{Tr}[\rho(\gamma)U^\dagger(\theta)O_iU(\theta)])_i$ , which we can engineer to both avoid barren plateaus and be robust against classical simulation. In this context, an absence of barren plateaus means that the final features show sufficient variation to produce new distinguishable data points.

The focus on this paper is more on the proposal of a generative model than its suitability for specific problems, which we leave to a future work. We do however, point out some features which we believe make it a promising area of investigation. Unlike other quantum generative models such as the Born machine [23–25] or quantum Boltzmann machine [26–28], the features are naturally continuous, which for NISQ devices is more practical than a binary discretization of continuous variables. We can also use parameter shift rules to calculate the gradient of these features with respect to the trainable variables, meaning our model could be utilised as the initial latent space, followed by subsequent classical neural network layers, in a more common generative model such as a generative adversarial network (GAN). In such cases, the quantum layer could be trained via the chain rule. This opens up the possibility of application to practically sized problems, something so far not possible with purely quantum generative models. Finally, the trainable layer is classically simulable, meaning that once a batch of quantum input data is generated, the update step could be calculated purely classically, exploiting techniques such as back-propagation; this would significantly speed-up the training of such models.

In Section II we explain the structure of our model and justification of our choices. In Section III we discuss the required criteria for trainability in terms of absence of barren plateau in trainable part as well as the condition we call subvolume law, showing that the generative part produces such states. In Section IV we look at two methods for classical simulation, tensor network contraction and Pauli propagation, and argue that our model poses difficulties for them. Finally in Section V, we go through the advantages of our model and provide some questions for further research.

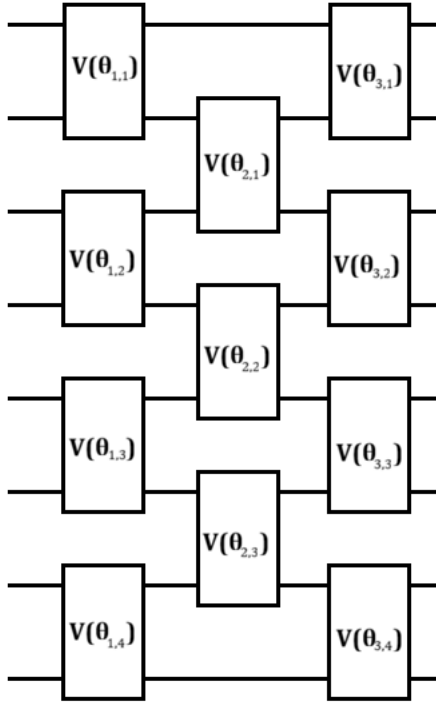


FIG. 2. The trainable part is composed of parametrized 2-qubit gates arranged in alternating pattern.

## II. MODEL STRUCTURE

### A. Model Outline

Our generative model circuits can be split into two distinct parts, as shown in Fig 1; a unitary whose parameters are chosen randomly with each run (the “generative circuit”) and a unitary whose parameters are initialised once and then trained (the “trainable circuit”). These two unitaries are run sequentially and, if using a shadow protocol, shadows would be taken after the application of the generative circuit, with the trainable circuit then being absorbed into the observables. The features of the model consists of expectation values of freely chosen  $k$ -local observables  $O_i$ , such as Pauli strings. Both choices of unitary are taken from circuit families known for not suffering from barren plateaus; small angle initialisation and shallow hardware efficient ansatz (HEA) respectively.

### B. The Trainable Circuit

Our primary goal is to choose for our trainable circuit family a  $V(\theta)$  that does not suffer from the problem of barren plateaus. As outlined in [29, 30], this is not merely a problem of choosing the right structure of  $V(\theta)$ , but requires choosing suitable operators  $O_i$ , as well the input states  $\rho(\gamma)$  (whose properties will depend on our choice of  $U(\gamma)$ , and will be discussed in the next section).

In addition to the absence of barren plateaus, we additionally desire that the observables can be evaluated classically (given a suitable classical description of the input state  $\rho(\gamma)$ ). This is not a property necessary for a useful quantum generative model, but rather motivated by the observation from [22] that the absence of barren plateaus often leads to such classical simulation, and the pragmatic view that classical training can take advantage of noiseless calculations, parallelism and back-propagation.

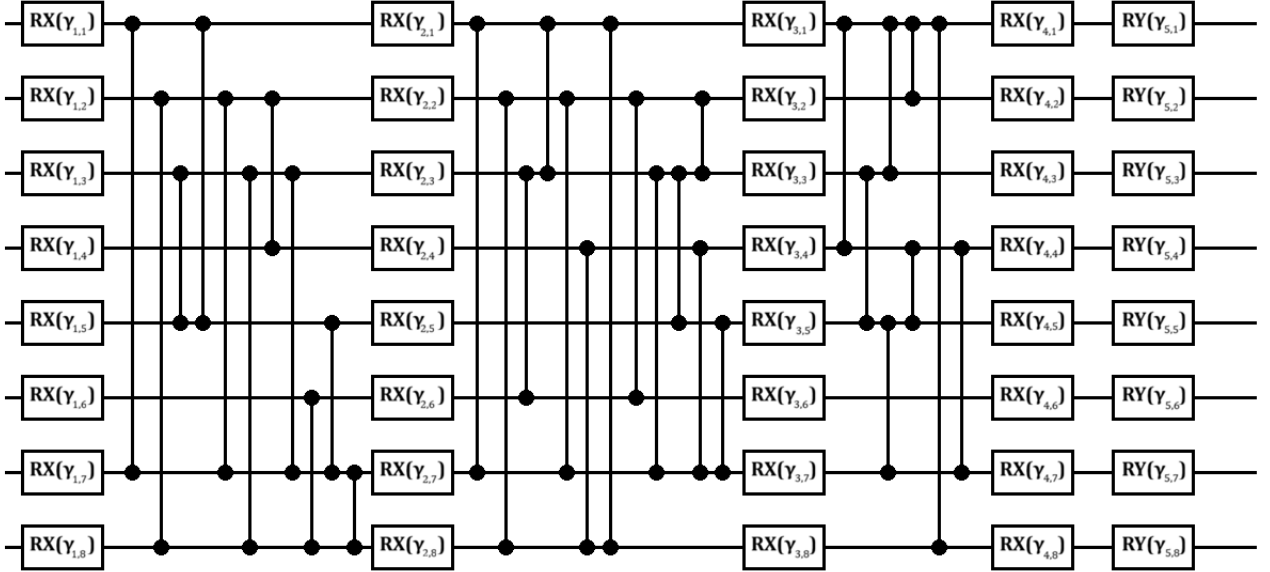


FIG. 3. The generative part has  $L$  layers with  $L = 3$  in the picture, each first applying parametrized  $X$ -rotations on each qubit followed by CZ gates between randomly chosen pairs of qubits. At the end both  $X$ - and  $Y$ -rotations are applied on each qubit.

We will choose our observables  $O_i$  to be  $k$ -local operators, and  $V(\theta)$  to be an HEA of depth  $\log n$ . Specifically, it consists of alternating layers of fully parameterised two qubit unitaries on neighbouring pairs of qubits on a 1d chain (the “brick layer ansatz”). With this ansatz, one can follow the “light cone” of a Heisenberg evolved operator  $V^\dagger(\theta)O_iV(\theta)$ , and see that it can only act non-trivially on  $2k \log n$  qubits, and is thus an element of a real Hilbert space of dimension  $4^{2k \log n} = n^{4k}$ . This element can be explicitly represented classically, and thus, when  $k$  is fixed, gives a polynomial (and thus classically efficient) description of our operator.

If we can obtain a classical description of  $\rho(\gamma)$  on the relevant  $2k \log n$  qubits, then we can update our  $\theta$  classically. This is exactly the use case that classical shadows [31] are useful for [14].

### C. The Generative Circuit

When choosing the circuit structure for our generative structure, we have two important conditions. Due to our choice of trainable circuit, the distribution  $P_\Gamma[\rho = \rho(\gamma)]$  should satisfy the weak subvolume law, described below, with high probability (preventing barren plateaus). Additionally, the reduced density matrices of  $\rho(\gamma)_\Lambda$  should not (with high probability) be possible to approximate classically efficiently. The second condition comes as a consequence of our operators  $V^\dagger(\theta)O_iV(\theta)$  being classically simulable; if we could additionally approximate  $\rho(\gamma)_\Lambda$  efficiently classically, our entire model could be evaluated classically, preventing any possible quantum advantage.

In addition to the above requirements, we also aim to make our circuit as amenable as possible to execution on real quantum hardware - in order to prevent classical simulation, we do not want to raise the bar too high for the quantum computer as well.

The structure we choose for our generative circuit consists of  $L = O(\log n)$  “layers”, each of which consists of a round of single  $R_X$  single qubit rotations with random angles  $\gamma_{i,l}$  independently drawn from Gaussian distribution of constant variance  $\tau^2$ , followed by CZ gates applied between some randomly chosen pairs of qubits. After these layers, a final round of  $R_X$  and then  $R_Y$  rotations to each qubit are applied. This is the same structure as studied in [21]. In principle we could choose any fixed 2-qubit gate that commutes with Pauli Z operator, but we select them to be CZ gates for the ease of analysis and implementation.

The properties of the states created by this model will depend heavily on the variance chosen and how the distribution defining the CZ gates; in order to satisfy our requirements above, we will choose the variance  $\tau^2$  of the RX rotation angles  $\gamma_{i,l}$  to be less than  $1/4$ , and the CZ gates in each layer to be drawn according to a  $G(n, p)$  Erdős–Rényi graph with  $p = \log(n)/n$ . In the following sections, we describe the justification for these choices in more detail, but we provide the intuition for them here briefly.

The variance is chosen to be constant size, which is as large as possible, whilst still ensuring that the distribution of states is polynomially distinguishable from the maximally mixed state on a subset of  $|\Lambda| = O(\log n)$  qubits, which is the relevant size for our trainable observable. It ensures, however, that the values of  $\sin(\gamma_{i,l})$  remain large enough to prevent one classical method of simulation, Pauli propagation, is unable to efficiently estimate the state  $\rho_\Lambda$ . This is because this algorithm propagates the observable through the Heisenberg evolution of the circuit in the Pauli basis, dropping terms with sufficiently small weight. These terms arise as a build up of  $\sin(\gamma_{i,l})$  terms when decomposing Pauli rotations; and thus larger angles can tolerate a higher number of sine terms before being dropped. Having  $k$  factors of  $\sin(\gamma_{i,l})$  makes the size of the coefficient  $(\tau^2)^k$  times smaller on average. The algorithm is ensured to obtain a polynomial precision if it keeps track of all terms with  $k \leq O(\log n)$  such sine factors, but this is a superpolynomial number of terms.

The CZ gates do not influence the provable absence of barren plateaus, but are chosen so that the light cone of a trainable observable is with high probability of macroscopic size; and that the connectivity graph captured by that light cone has a tree-width of  $\Theta(n)$ . This prevents efficient classical approximation via tensor network techniques which, along with Pauli propagation, are the two most effective classical techniques for small-angle circuits. Furthermore the individual CZ layers are sufficiently sparse, such that with high probability, they can be transpiled onto a square grid architecture with depth  $O(\sqrt{n} \log n)$ . This sublinear scaling is promising for experiments run on NISQ devices. [32] This choice is a compromise between having denser CZ graphs to make tensor network contraction harder and sparser graphs being easier to implement physically.

These choices ensure that our generative circuit gives sufficient detectable variation to the trainable circuit to be of use in a generative model; whilst remaining robust against the two best-known classical simulation techniques. This makes it a prime candidate to provide something genuinely quantum in the field of generative learning.

### III. AVOIDING BARREN PLATEAUS

#### A. Area Law vs Subvolume Law

The standard definition of the area law for the entanglement from quantum many-body physics requires that for a subsystem  $\Lambda$  the entropy of entanglement, i.e. the von Neumann entropy of the reduced density matrix, scales with the size of the boundary, i.e.

$$S(\rho_\Lambda) := -\text{Tr}[\rho_\Lambda \log \rho_\Lambda] \sim |\partial\Lambda| \quad (1)$$

For a volume law, one instead has that the entropy scales with the size,  $S(\rho_\Lambda) \sim |\Lambda|$ . In the barren plateau literature, the relevant quantity is the distance of the reduced density matrix from the maximally mixed state. This leads to different definitions: an area law requires  $|\Lambda| - S(\rho_\Lambda) \geq 1/\text{poly}(n)$  and a volume law  $|\Lambda| - S(\rho_\Lambda) \leq 1/\exp(n)$ .

To avoid confusion related to these terms, we shall adopt following convention. We say that a state  $\rho$  possesses *subvolume law* for the entanglement within  $\Lambda$  if

$$S(\rho_\Lambda) \in o(|\Lambda|), \quad (2)$$

and it possesses *weak subvolume law* if

$$S(\rho_\Lambda) \leq |\Lambda| - \frac{1}{P(n)} \quad (3)$$

for a polynomial  $P$ . The definition for weak subvolume law coincides with the definition of area law in barren plateau literature. Note that subvolume law implies weak subvolume law.

An information theoretical measure of pure state entanglement is distinguishability of a subsystem from maximally mixed state

$$\mathcal{I}_\Lambda(\rho) := \|\rho_\Lambda - \frac{1}{2^{|\Lambda|}} \text{Id}\|_1, \quad (4)$$

where the norm is taken to be the Schatten 1-norm, the sum of singular values. For any observable  $O$  acting non-trivially on  $\Lambda$ , we have that  $|\text{tr}(O\rho) - 2^{-n}\text{Tr}[O]| \leq \mathcal{I}_\Lambda(\rho)\|O\|_\infty$ .

Using the continuity of entropy and the fact that the maximum at maximally mixed state is a critical point, we see that when  $|\Lambda| \in O(\log n)$  the state possesses weak subvolume law within  $\Lambda$  if and only if  $\mathcal{I}_\Lambda(\rho) \in \Omega(1/\text{poly}(n))$ . By Taylor expansion around the critical point, we see that  $|\Lambda| - S(\rho_\Lambda) \sim \|\rho_\Lambda - \frac{1}{2^{|\Lambda|}} \text{Id}\|_2^2$  in Hilbert-Schmidt distance, and for logarithmic  $|\Lambda|$  the Schatten 1-norm is equivalent to the 2-norm up to a polynomial factor.

## B. The connection of weak subvolume law and absence of barren plateaus

In order for circuit to be trainable, we want that the gradient of the cost function is large, meaning  $|\nabla f| \geq 1/\text{poly}(n)$ , for large portion of the parameter space. To ensure this, one needs a lower bound on partial derivatives.

Theorem 2 in [10] gives a lower bound for the variance of partial derivatives for the cost function  $f = \sum_i c_i \text{Tr}[U^\dagger O_i U \rho]$  as

$$\text{Var}(\partial_\nu f) \geq c^D \sum_{i \in i_{\mathcal{L}}} \sum_{(k, k') \in k_{\mathcal{L}_B}} c_i^2 \epsilon(\rho_{k, k'}) \epsilon(O_i), \quad (5)$$

where  $O_i$  are acting on qubits in the forward light cone, the subsystems  $(k, k')$  are contained in the backward light cone, and  $\epsilon(A) := \|A - \text{tr}(A)\text{Id}/\dim(A)\|_2$  is Hilbert-Schmidt distance from normalized identity.

Here we see the role of entanglement: if one of the  $\epsilon(\rho_{k, k'})$  is polynomially large, then the variance of the partial derivative is polynomially large and we have no barren plateau. Using the relation between norms we obtain the bound  $\epsilon(\rho_{k, k'}) \geq 2^{-|(k, k')|} \mathcal{I}_{(k, k')}(\rho)$ , and we see that the weak subvolume law on logarithmic subsystems of the initial state implies absence of barren plateaus for HEA - as the assumption that the circuit is of logarithmic depth, and the final observable is local, means the prefactor scales polynomially with  $n$ .

## C. Small angle initialized state satisfies subvolume law

For the HEA as our trainable part, there are three scenarios that can cause exponential concentration of the observable. If the circuit is too deep or the observable is global, then we run into barren plateaus: the gradient is exponentially small for most parameter values. It is for this reason we assume that the circuit depth is logarithmic and the observable is a sum of Pauli operators supported on a constant number of qubits. This leaves us to consider the third way that can lead to barren plateaus - if the initial state is too highly entangled.

Our proof showing an absence of barren plateaus for our model follows closely the argument in [21]; however, we are able to strengthen the result by adding an additional logarithmic factor in the variance. This is possible because instead of using the estimate  $(1 - 1/M)^M \geq c$  in the proof we use  $(1 - a/M)^M = (1 - a/M)^{a(M/a)} \geq c^a$ , where we have  $a = \log n$ . We show that a circuit with small angle initialization as introduced in Section 4.1 of [21] produces states that satisfy subvolume law.

The circuit  $V(\theta)$  consists of layers that perform single qubit rotations and layers of some CZ gates. After a total of  $2L$  such alternating layers, there is a layer of  $X$ -rotations and a layer of  $Y$ -rotations. This structure is illustrated earlier in Fig 3. We write each single qubit rotation as  $R(\gamma_{l,n}) = e^{-i\gamma_{l,n} G_{l,n}}$ . Let every  $G_{l,n}$  be Hermitian unitaries that anti-commute with  $\sigma_3$  (a Z-gate).

**Theorem** Assume that  $\gamma_{l,n} \sim \mathcal{N}(0, \tau^2)$  are independent and identically distributed, where  $\tau^2 := \frac{\log n}{16S(L+2)}$  for a constant  $S$ . Let  $\rho = \rho(\gamma)$  be the state obtained by applying  $V(\gamma)$  to the all zeroes state  $|0\rangle$ . Then for any subsystem  $\Lambda$  with  $|\Lambda| = O(\log n)$ , we have that the expectation of the square of distinguishability between reduced state  $\rho_\Lambda = \rho_\Lambda(\gamma)$

and maximally mixed state  $\frac{1}{2^{|\Lambda|}}\text{Id}$  is polynomially large, i.e.

$$\mathbb{E} \left\| \rho_\Lambda - \frac{1}{2^{|\Lambda|}}\text{Id} \right\|_1^2 = \Omega(1/\text{poly}(n)). \quad (6)$$

Above the norm is the trace norm, also known as Schatten 1-norm.

To prove this, we use the duality of Schatten norm  $\|S\|_1 = \sup\{|\text{Tr}(ST^\dagger)| : \|T\|_\infty = 1\}$ . In particular, letting  $\sigma = \sigma_\Lambda \otimes \text{Id}$  be a Pauli operator acting non-trivially on  $S$  qubits on  $\Lambda$ , we have

$$\mathbb{E} \|\rho_\Lambda - \frac{1}{2^{|\Lambda|}}\text{Id}\|_1^2 \geq \mathbb{E} \text{Tr}(\sigma_\Lambda(\rho_\Lambda - \frac{1}{2^{|\Lambda|}}\text{Id}))^2 = \mathbb{E} \text{Tr}(\sigma_\Lambda \rho_\Lambda)^2 = \mathbb{E} \text{Tr}(\sigma \rho)^2. \quad (7)$$

We use the following lemma (Lemma B.1 from [21]) iteratively to estimate the expectation.

**Lemma.** Let  $\gamma$  be a variable with Gaussian distribution  $\mathcal{N}(0, \tau^2)$ . Let  $\rho = \sum_k c_k \rho_k$  be the linear combination of density matrices  $\{\rho_k\}$  with real coefficients  $\{c_k\}$ . Let  $G$  be a Hermitian unitary and  $V = e^{-i\gamma G}$ . Let  $O$  be an arbitrary Hermitian quantum observable that anti-commutes with  $G$ . Then

$$\mathbb{E} \text{Tr}[OV\rho V^\dagger]^2 \geq (1 - 4\tau^2) \text{Tr}[O\rho]^2 + 4\tau^2(1 - 4\tau^2) \text{Tr}[iGO\rho]^2. \quad (8)$$

Let  $\rho_l$  be the density matrix after  $l$  layers, where each of the first  $L$  layers consists of rotations and one layers of CZ operations. Let  $\tilde{\sigma}$  be the Pauli operator that is obtained by replacing  $\sigma_1$  with  $\sigma_3$  at every index in  $\sigma$ . Then

$$\begin{aligned} & \mathbb{E}_{\gamma_1} \mathbb{E}_{\gamma_2} \cdots \mathbb{E}_{\gamma_{L+2}} \text{Tr}[\sigma \rho_{L+2}]^2 \\ &= \mathbb{E}_{\gamma_1} \mathbb{E}_{\gamma_2} \cdots \mathbb{E}_{\gamma_{L+1}} \mathbb{E}_{\gamma_{L+2}} \text{Tr}[\sigma R_{L+2}(\gamma_{L+2}) \rho_{L+1} R_{L+2}(\gamma_{L+2})^\dagger]^2 \\ &\geq \mathbb{E}_{\gamma_1} \mathbb{E}_{\gamma_2} \cdots \mathbb{E}_{\gamma_{L+1}} [4\tau^2(1 - 4\tau^2)]^{S_1} (1 - 4\tau^2)^{S_3} \text{Tr}[\tilde{\sigma} \rho_{L+1}]^2, \end{aligned}$$

where we used the fact that  $Y$ -rotations commute with  $\sigma_2$ . We denote by  $S_j$  the number of times the operation  $\sigma_j$  appear in  $\sigma$ , noting that  $S_1 + S_2 + S_3 = S$ . Let  $\sigma'$  be the Pauli operator obtained from  $\sigma$  by replacing with  $\sigma_3$  at all indices where  $\sigma$  acts non-trivially. Then

$$\begin{aligned} & \mathbb{E}_{\gamma_1} \mathbb{E}_{\gamma_2} \cdots \mathbb{E}_{\gamma_{L+1}} [4\tau^2(1 - 4\tau^2)]^{S_1} (1 - 4\tau^2)^{S_3} \text{Tr}[\tilde{\sigma} \rho_{L+1}]^2 \\ &\geq \mathbb{E}_{\gamma_1} \mathbb{E}_{\gamma_2} \cdots \mathbb{E}_{\gamma_L} [4\tau^2(1 - 4\tau^2)]^{S_1 + S_2} (1 - 4\tau^2)^{S_1 + 2S_3} \text{Tr}[\sigma' \rho_L]^2 \\ &\geq \mathbb{E}_{\gamma_1} \mathbb{E}_{\gamma_2} \cdots \mathbb{E}_{\gamma_L} [4\tau^2(1 - 4\tau^2)]^S (1 - 4\tau^2)^S \text{Tr}[\sigma' \rho_L]^2. \end{aligned}$$

Using the fact that CZ-gates commute with  $\sigma'$ , we can apply the lemma iteratively to estimate that

$$\begin{aligned} & \mathbb{E}_{\gamma_1} \mathbb{E}_{\gamma_2} \cdots \mathbb{E}_{\gamma_L} [4\tau^2(1 - 4\tau^2)]^S (1 - 4\tau^2)^S \text{Tr}[\sigma' \rho_L]^2 \\ &= \mathbb{E}_{\gamma_1} \mathbb{E}_{\gamma_2} \cdots \mathbb{E}_{\gamma_L} [2\tau(1 - 4\tau^2)]^{2S} \text{Tr}[\sigma' \rho_L]^2 \\ &\geq \mathbb{E}_{\gamma_1} \mathbb{E}_{\gamma_2} \cdots \mathbb{E}_{\gamma_{L-1}} [2\tau(1 - 4\tau^2)]^{2S} (1 - 4\tau)^S \text{Tr}[\sigma' \rho_{L-1}]^2 \\ &\geq [2\tau(1 - 4\tau^2)]^{2S} (1 - 4\tau)^S \text{Tr}[\sigma' \rho_0]^2 \\ &= (4\tau^2)^S (1 - 4\tau^2)^{S(L+2)} \text{Tr}[\sigma' \rho_0]^2 \\ &= \frac{(\log n)^S}{(4S)^S (L+2)^S} \left(1 - \frac{\log n}{4S(L+2)}\right)^{S(L+2)} \text{Tr}[\sigma' \rho_0]^2 \\ &\geq \frac{1}{(4S)^S (L+2)^S} \left(1 - \frac{1}{2}\right)^{2(\log n/4)} \text{Tr}[\sigma' \rho_0]^2. \end{aligned}$$

As the initial state is all zeroes,  $S$  is a constant and  $L$  is subpolynomial in  $n$ , this proves that the distinguishability is bounded below by  $1/\text{poly}(n)$ . It follows that the combined circuit does not suffer from barren plateau.

Note that we have essentially combined two methods that avoid barren plateaus, small angle initialization and shallow HEA, into one. In principle, one needs expectations on subsystems up to logarithmic size on the small angle part in order to simulate the system.

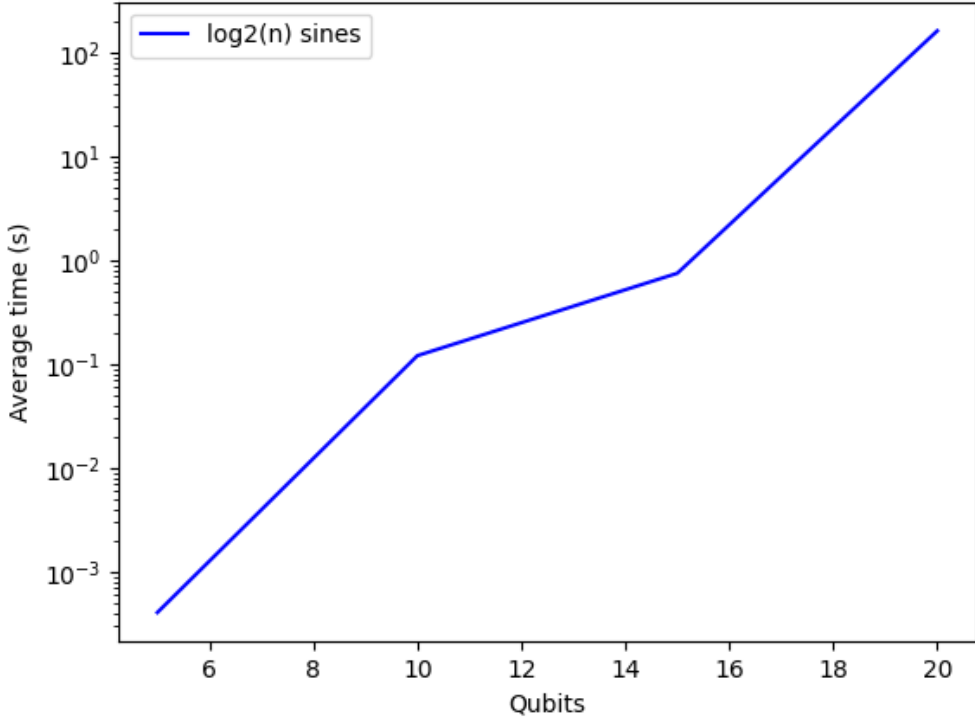


FIG. 4. The average running time of Pauli propagation algorithm on a laptop with cutoff at  $\lceil \log_2(n) \rceil$  sine factors.

## IV. CLASSICAL SIMULATION METHODS

### A. Pauli Propagation

In order to understand how we choose our circuit to be difficult for Pauli propagation, we first outline how it works. Pauli propagation is based on the idea of tracking observables written as Pauli sums  $O = \sum_j c_j P_j$  through the circuit. In each step of the algorithm, the current Pauli sum is conjugated by the current gate, yielding the sum for the next step. For a Clifford gate  $C$ , all Pauli strings are mapped to Pauli strings as  $CPC^\dagger = P'$ . For a single qubit Pauli rotation  $R(\gamma)$ , all Pauli strings that commute with it stay the same, while those Pauli strings  $P$  that do not are taken to  $R(\gamma)PR(\gamma)^\dagger = \cos(\gamma)P + \sin(\gamma)P'$ . This produces two new strings to keep track of.

Though the number of terms in the sum grows exponentially, an approximation algorithm obtained by truncating terms is reasonable to compute classically. The truncation drops the terms with coefficients of small absolute value or ones that have large number of non-identities in Pauli strings, and the total error is small when the angles of the circuit are small. [33]

Because the Pauli propagation is well-suited for small-angle circuits, our choice of circuit should try to minimize its effectiveness. For a quantum circuit, finding expectation of an observable up to polynomially small error takes polynomial time, and therefore we set the goal of Pauli propagation to be finding the expectation up to polynomial error. The estimates from [33] for resources taken by Pauli propagation indicate that this would take quasipolynomial running time  $O(n^{\log n})$ , and we explain below the justification for why poor scaling is expected.

In our model, the angles of the single qubit rotations are drawn from a Gaussian distribution with constant variance. This means that the relative error from truncating terms after constant number of sine factors is constant, and getting a polynomially scaling truncation error requires keeping track of terms with logarithmic number of sine factors. As there is superpolynomial number of such terms, the Pauli propagation algorithm cannot run in polynomial time. We show the running time for small number of qubits in Figure 4.

If the truncation is instead performed on terms with large number of non-identity Pauli operators, then it can be easily seen that if we truncate terms with constant number of such operators, we may lose terms in the final step of the algorithm that contribute polynomially to the expectation. If logarithmic number of non-identities are permitted before truncation, the number of kept terms would again be superpolynomially large. We suspect that a specific combination of these two extremes may be more efficient: an algorithm that would increase the number of kept terms near the end.

## B. Tensor Network Simulation

Another strategy for simulating quantum systems classically is based on contracting tensor networks. Tensors generalize matrices: a tensor is a multidimensional array, and contracting tensors creates a new tensor by summing over shared indices analogously to matrix product. A quantum system can be represented as a tensor network: a set of tensors with rules for contracting them. The order in which the contractions are performed impact heavily the complexity of the contraction.

Approximate approaches using tensor networks such as matrix product states and operators (MPS/MPO) and projected entangled pair states (PEPS) have had great success in a wide range of simulations of quantum systems. For an introduction into these methods, see [34]. These methods produce efficient approximations when entanglement of the system is limited, particularly in case of the area law states seen in many-body physics. Since our proof of an absence of a barren plateau relies on a limited subsystem entanglement, we should consider whether these tensor network techniques are suitable for simulating our model.

From the perspective of tensor network simulation, the tensor network to contract corresponds to the expectation value  $\langle \Phi(\gamma) | \tilde{O} | \Phi(\gamma) \rangle$ , where  $|\Phi(\gamma)\rangle = U(\gamma) |0\rangle^{\otimes n}$  and  $\tilde{O}$  is an observable with non-trivial support on  $2k \log n$  qubits (either  $V^\dagger(\theta) O_i V(\theta)$ , or one of the  $2k \log n$  length Pauli strings to describe the relevant reduced state). This provides us with a tensor network we need to contract into a single value whose properties we can look at to determine its difficulty. Only gates in  $U(\gamma)$  which appear in the light cone of  $\tilde{O}$  need be considered, as other gates cancel out during the contraction.

As a tree decomposition of the network graph can be used to obtain a contraction order, the best possible complexity of the contraction depends on the treewidth of the graph [35]. We denote by  $G_l$  the graph on  $n$  vertices corresponding to the qubits, with edges between those vertices where there is a CZ gate between qubits in  $l$ th layer of the generative circuit. As single qubit gates do not affect the treewidth of the tensor network, the choice of CZ gates according to graphs  $G_l$  in each layer completely determine the final treewidth. Moreover, all the gates outside the relevant light cone can be made to cancel out during the contraction by using the fact that CZ gates commute with each other, and therefore we need to reach a high treewidth inside that light cone to ensure difficulty. Our strategy is to choose our graphs  $G_l$  such that the following are true:

- After going back through layers  $l = 2 \dots L$ , all  $n$  qubits are in the light cone with high probability.
- The graph  $G_1$  has a treewidth of  $\Theta(n)$  with high probability.

This will ensure that with high probability  $G_1$  is a subgraph of our tensor network, and thus provides a lower bound for the treewidth.

Our approach is inspired by [32], who consider placement of diagonal 2-qubit gates for a different purpose, relating to the anti-concentration of Instantaneous Quantum Polynomial (IQP) circuits. At each layer we take  $G_l$  to be a  $G(n, p)$  Erdős-Rényi graph with  $p = \log(n)/n$ . One can see the expected number of 2 qubits gates acting on a single qubit is  $\sim \log n$ , with the expected total number of 2 qubits  $\sim n \log n$ .

We now sketch the relevant properties of our circuit that these graphs provide. The first concerns the spread of the light cone. If the expected number of connections for a single node is  $c$ , then in  $L = \log_c n$  layers we expect to have discovered  $\Theta(n)$  nodes (at each step we expect to discover  $c$  new nodes from each of our old nodes, with duplicates only becoming an issue as we approach macroscopic scales). Thus with  $L = \log(n)/\log(\log(n))$  we expect to have seen  $\Theta(n)$  of the qubits - we will however take  $L = \log(n)$ , to increase this further.

Now our lightcone is of the order  $\Theta(n)$ , we can consider the tree width  $W_{\text{tree}}$  of our random graph in the first layer,  $G_1$ . Here we use a result from [36], which states for  $G(n, p)$  graphs that  $W_{\text{tree}}(G) = n - o(n)$  if  $p$  grows faster than

$c/n, c > 1$ . Thus we can be sure that the tree width of our tensor network contraction is at least as large as  $\Theta(n)$ , ensuring exponential scaling.

We note that, to obtain both these properties, it would have been sufficient to take  $p = c/n, c > 1$  instead, keeping  $L = \log n$ . However, layers of our chosen form can be transpiled onto a square grid architecture with depth  $\sqrt{n} \log(n)$  with high probability; resulting in a total depth of  $O(\sqrt{n} \log^2(n))$ . We feel that the extra factor of  $\log(n)$  in the depth is worth the extra difficulty that results in the tensor network contraction, though we admit an alternative trade-off may be possible.

## V. CONCLUSIONS AND FURTHER DIRECTIONS

The quantum generative model we have proposed in this paper has two parts. The generative part of the circuit has  $L = O(\log n)$  layers of Pauli  $x$ -rotations applied to each qubit with angles drawn from  $\mathcal{N}(0, 1/4)$ , each rotation layer followed by some CZ gates, applied between each pair of qubits with probability  $(\log n)/n$ . At the end of the generative part, there are additional  $X$ - and  $Y$ -rotations applied to all qubits. In the trainable part, parametrized 2-qubit gates are applied between neighbouring qubits on a line in alternating pattern, keeping the depth logarithmic. Our model thus essentially combines a small angle initialization with an HEA. The features of the model are expectations of local observables.

The model has many promising qualities. First of all, we have shown that it does not suffer from barren plateaus. Since the trainable part of our model can be done classically, the issue of barren plateaus in this context becomes one of being able to distinguish between the random instances providing variation in the generative model. We can therefore associate a barren plateau with generative modelling problem of “mode collapse”. Moreover, we have aimed to make classical simulation by tensor networks and Pauli propagation as hard as possible within the constraints introduced by our proof. For tensor networks, the randomized choice of CZ gates means that the connectivity is non-local, making the state difficult to approximate with MPS, and the depth choice makes the treewidth of the circuit large. As for Pauli propagation, constant size of the rotation angles means that the error from truncation is not guaranteed to be small for usual choices of truncation criteria.

The generative part of the circuit introduces randomness obtained by randomly choosing a quantum circuit. The features of the model are continuous, which can be considered a better alternative to expressing floating point numbers in binary with small number of qubits on NISQ devices. Finally, training the model can be done by using parameter shift rule, and it can be done with a classical computer provided that a quantum experiment is performed beforehand to find classical shadows. We believe the model to be interesting to anyone seeking to push the boundaries of theory surrounding barren plateaus and that it inspires new ideas.

We believe there are still some important questions to answer to understand the consequences of this model, namely:

- As we have shown, the model avoids barren plateaus in noiseless setting. However, we know from [37] that noise can induce barren plateau to an ansatz while the noiseless version does not suffer from one. It is therefore important to understand, how robust the model is to noise.
- Some of the choices we made in the structure of the model could be made differently. For example, the sparse all-to-all graphs of CZ gates in the generative part could be changed to some other structure, such square grid connections, in order to make the circuit easier to implement on a real hardware. As a trade-off, we would need to increase the number of layers to reach large treewidths for tensor networks, and therefore would have to decrease the angle size in the single qubit rotations to avoid running into barren plateaus. Additionally, we could replace CZ gates with other entangling gates, as long as they commute with the Pauli Z-operators. It is currently unclear how that would affect the difficulty of simulating the model, especially in regards to Pauli propagation, which currently benefits from the CZ gates being Clifford.
- We have only considered tensor networks and Pauli propagation when we argued for hardness. In light of [22], is there a more efficient classical simulation strategy? One possible approach could be a version of Pauli propagation that dynamically truncates less at later steps.

---

[1] P. W. Shor, *SIAM Journal on Computing* **26**, 1484 (1997).

[2] J. Preskill, *Quantum* **2**, 79 (2018).

[3] M. Cerezo, A. Arrasmith, R. Babbush, S. C. Benjamin, S. Endo, K. Fujii, J. R. McClean, K. Mitarai, X. Yuan, L. Cincio, and P. J. Coles, *Nature Reviews Physics* **3**, 625–644 (2021).

[4] M. Stęchly, “Introduction to variational quantum algorithms,” (2024), [arXiv:2402.15879 \[quant-ph\]](https://arxiv.org/abs/2402.15879).

[5] S. Jerbi, L. J. Fiderer, H. P. Nautrup, J. M. Kübler, H. J. Briegel, and V. Dunjko, *Nature Communications* **14** (2023).

[6] J. M. McClean, S. Boixo, V. N. Smelyanskiy, R. Babbush, and H. Neven, *Nature Communications* **9**, 4812 (2018).

[7] H. Qi, L. Wang, H. Zhu, A. Gani, and C. Gong, *Quantum Information Processing* **22**, 435 (2023).

[8] A. Arrasmith, Z. Holmes, M. Cerezo, and P. J. Coles, *Quantum Science and Technology* **7**, 045015 (2022).

[9] M. Larocca, S. Thanasisilp, S. Wang, K. Sharma, J. Biamonte, P. J. Coles, L. Cincio, J. R. McClean, Z. Holmes, and M. Cerezo, “A review of barren plateaus in variational quantum computing,” (2024), [arXiv:2405.00781 \[quant-ph\]](https://arxiv.org/abs/2405.00781).

[10] M. Cerezo, A. Sone, T. Volkoff, L. Cincio, and P. J. Coles, *Nature Communications* **12**, 1791 (2021).

[11] S. Khatri, R. LaRose, A. Poremba, L. Cincio, A. T. Sornborger, and P. J. Coles, *Quantum* **3**, 140 (2019).

[12] C. Zhao and X.-S. Gao, *Quantum* **5**, 466 (2021).

[13] Z. Liu, L.-W. Yu, L.-M. Duan, and D.-L. Deng, *Physical Review Letters* **129**, 270501 (2022).

[14] A. Basheer, Y. Feng, C. Ferrie, and S. Li, *Proceedings of the AAAI Conference on Artificial Intelligence* **37**, 6770–6778 (2023).

[15] A. Letcher, S. Woerner, and C. Zoufal, *Quantum* **8** (2024).

[16] Y. Suzuki and M. Li, *Phys. Rev. A* **110**, 012409 (2024).

[17] L. Leone, S. F. Oliviero, L. Cincio, and M. Cerezo, *Quantum* **8**, 1395 (2024).

[18] A. Pesah, M. Cerezo, S. Wang, T. Volkoff, A. T. Sornborger, and P. J. Coles, *Physical Review X* **11**, 041011 (2021).

[19] C.-Y. Park and N. Killoran, [arXiv preprint arXiv:2302.08529](https://arxiv.org/abs/2302.08529) (2023).

[20] Y. Wang, B. Qi, C. Ferrie, and D. Dong, *Phys. Rev. Appl.* **22**, 054005 (2024).

[21] K. Zhang, L. Liu, M.-H. Hsieh, and D. Tao, *Advances in Neural Information Processing Systems* **35**, 18612 (2022).

[22] M. Cerezo, M. Larocca, D. García-Martín, N. L. Diaz, P. Braccia, E. Fontana, M. S. Rudolph, P. Bermejo, A. Ijaz, S. Thanasisilp, E. R. Anschuetz, and Z. Holmes, *Nature Communications* **16**, 7907 (2025).

[23] S. Cheng, J. Chen, and L. Wang, *Entropy* **20**, 583 (2018).

[24] J.-G. Liu and L. Wang, *Phys. Rev. A* **98**, 062324 (2018).

[25] M. Benedetti, D. Garcia-Pintos, O. Perdomo, V. Leyton-Ortega, Y. Nam, and A. Perdomo-Ortiz, *npj Quantum Information* **5**, 45 (2019).

[26] M. H. Amin, E. Andriyash, J. Rolfe, B. Kulchytskyy, and R. Melko, *Phys. Rev. X* **8**, 021050 (2018).

[27] M. Kieferová and N. Wiebe, *Phys. Rev. A* **96**, 062327 (2017).

[28] M. Benedetti, J. Realpe-Gómez, R. Biswas, and A. Perdomo-Ortiz, *Phys. Rev. X* **7**, 041052 (2017).

[29] M. Ragone, B. N. Bakalov, F. Sauvage, A. F. Kemper, C. O. Marrero, M. Larocca, and M. Cerezo, *Nature Communications* (2024).

[30] E. Fontana, D. Herman, S. Chakrabarti, N. Kumar, R. Yalovetzky, J. Heredge, S. H. Sureshbabu, and M. Pistoia, *Nature Communications* (2024).

[31] H. Huang, R. Kueng, and J. Preskill, *Nature Physics* **16**, 1050 (2020).

[32] M. J. Bremner, A. Montanaro, and D. J. Shepherd, *Quantum* **1**, 8 (2017).

[33] S. Lerch, R. Puig, M. S. Rudolph, A. Angrisani, T. Jones, M. Cerezo, S. Thanasisilp, and Z. Holmes, [arXiv:2411.19896 \[quant-ph\]](https://arxiv.org/abs/2411.19896).

[34] J. C. Bridgeman and C. T. Chubb, *Journal of Physics A: Mathematical and Theoretical* **50**, 223001 (2017).

[35] I. L. Markov and Y. Shi, *SIAM Journal on Computing* **38**, 963 (2008), <https://doi.org/10.1137/050644756>.

[36] C. Wang, T. Liu, P. Cui, and K. Xu, in *Combinatorial Optimization and Applications*, edited by W. Wang, X. Zhu, and D.-Z. Du (Springer Berlin Heidelberg, Berlin, Heidelberg, 2011) pp. 491–499.

[37] S. Wang, E. Fontana, M. Cerezo, K. Sharma, A. Sone, L. Cincio, and P. J. Coles, *Nature Communications* **12** (2021), [10.1038/s41467-021-27045-6](https://doi.org/10.1038/s41467-021-27045-6).